c-Met PET Imaging Detects Early-Stage Locoregional Recurrence of Basal-Like Breast Cancer

Appitha Arulappu*[1], Mark Battle*[2], Michel Eisenblaetter*[1,3,4], Graeme McRobbie[2], Imtiaz Khan[2], James Monypenny[1], Gregory Weitsman[1], Myria Galazi[1], Susan Hoppmann[2], Patrycja Gazinska[5], Wulan Wulaningsih[1], Grethe Tang Dalsgaard[2], Sven Macholl†[2,6], and Tony Ng†[1,5,7]

[1]*Richard Dimbleby Department of Cancer Research, Kings College London, London, United Kingdom;* [2]*GE Healthcare, Life Sciences, Amersham, United Kingdom;* [3]*Division of Imaging Sciences & Biomedical Engineering, King's College London, London, United Kingdom;* [4]*Department of Clinical Radiology, University Hospital Münster, Münster, Germany;* [5]*Breast Cancer NOW Unit, King's College London School of Medicine, London, United Kingdom;* [6]*Barts Cancer Institute, Queen Mary University of London, London, United Kingdom; and* [7]*UCL Cancer Institute, University College London, London, United Kingdom*

Locoregional recurrence of breast cancer poses significant clinical problems because of frequent inoperability once the chest wall is involved. Early detection of recurrence by molecular imaging agents against therapeutically targetable receptors, such as c-Met, would be of potential benefit. The aim of this study was to assess ^{18}F-AH113804, a peptide-based molecular imaging agent with high affinity for human c-Met, for the detection of early-stage locoregional recurrence in a human basal-like breast cancer model, HCC1954. **Methods:** HCC1954 tumor–bearing xenograft models were established, and ^{18}F-AH113804 was administered. Distribution of radioactivity was determined via PET at 60 min after radiotracer injection. PET and CT images were acquired 10 d after tumor inoculation, to establish baseline distribution and uptake, and then on selected days after surgical tumor resection. CT images and caliper were used to determine the tumor volume. Radiotracer uptake was assessed by ^{18}F-AH113804 PET imaging. c-Met expression was assessed by immunofluorescence imaging of tumor samples and correlated with ^{18}F-AH113804 PET imaging results. **Results:** Baseline uptake of ^{18}F-AH113804, determined in tumor-bearing animals after 10 d, was approximately 2-fold higher in the tumor than in muscle tissue or the contralateral mammary fat pad. The tumor growth rate, determined from CT images, was comparable between the animals with recurrent tumors, with detection of tumors of low volume ($<$10 mm^3) only possible by day 20 after tumor resection. ^{18}F-AH113804 PET detected local tumor recurrence as early as 6 d after surgery in the recurrent tumor–bearing animals and exhibited significantly higher ^{18}F-AH113804 uptake (in comparison to mammary fatty tissue), with a target-to-background (muscle) ratio of approximately 3:1 ($P < 0.01$). The c-Met expression of individual resected tumor samples, determined by immunofluorescence, correlated with the respective ^{18}F-AH113804 imaging signals ($r = 0.82$, $P < 0.05$). **Conclusion:** ^{18}F-AH113804 PET provides a new diagnostic tool for the detection of c-Met–expressing primary tumor and has potential utility for the detection of locoregional recurrence from an early stage.

Received Jul. 26, 2015; revision accepted Nov. 13, 2015.

For correspondence or reprints contact: Tony Ng, The Richard Dimbleby Department of Cancer Research, New Hunt's House, Guy's Hospital Campus, London SE1 1UL, UK.

E-mail: tony.ng@kcl.ac.uk

*Contributed equally to this work.

†Contributed equally to this work.

Published online Dec. 3, 2015.

Key Words: PET/CT imaging; basal-like breast cancer; HCC1954; c-Met; AH113804; cancer; loco-regional recurrence

J Nucl Med 2016; 57:765–770
DOI: 10.2967/jnumed.115.164384

The protooncogene c-Met is a receptor tyrosine kinase activated by the ligand hepatocyte growth factor. The hepatocyte growth factor/c-Met signaling axis has been described as a promoter of cancer cell growth, angiogenesis, invasion, and metastasis (*1*). Overexpression of c-Met is associated with poor prognosis and a more malignant tumor phenotype (*2,3*). Several c-Met inhibitors are currently under evaluation in clinical trials, either as stand-alone therapies or in concomitant treatment (*4*). c-Met is overexpressed in various solid tumors (*5*), including breast cancer (BC), with higher expression in basal-like BC (BLBC) than in other intrinsic cancer subtypes (*6*). BLBC, which accounts for up to 15% of all BCs, exhibits a high rate of locoregional recurrence after initial therapy (*7–10*).

Although treatment of localized disease has improved over the past decades, up to 45% of BC patients suffer a local, regional, or systemic relapse within 8 y after initial therapy (*8*). Although systemic relapse in the form of distant metastasis is still regarded as incurable according to current treatment guidelines, locoregional recurrence of BC should be treated with curative intention (*11*). Treatment success crucially depends on the earliest possible diagnosis, before chest wall involvement or further organ invasion prevents any form of aggressive treatment (*12*). Established guidelines for posttherapy monitoring in BLBC feature mammography and clinical examination, which frequently fail to identify local tumor relapse at a sufficiently early stage (*13*).

MRI and ^{18}F-FDG PET/CT offer a comparably higher sensitivity and specificity for detection and characterization of BC relapse (*14*). However, differentiation of recurrent BC from inflammatory or infectious processes and the identification of small lesions (tumor size $<$ 20 mm) still impose challenges for ^{18}F-FDG PET (*15,16*). c-Met–targeted imaging could provide such a tool to further improve the performance of posttreatment surveillance and could aid patient stratification for targeted therapy.

For this study, we chose the novel, peptide-based molecular imaging agent ^{18}F-AH113804 (Fig. 1A), which binds to human c-Met with

high affinity (*Kd* ≈ 2 nM), has a favorable kinetic profile, exhibits specific uptake in c-Met–positive tumor tissue, and rapid systemic clearance (*17*). These advantageous properties of ^{18}F-AH113804 enable diagnostic PET imaging as early as 1 h after administration (*17*). The safety, pharmacokinetics, and imaging characteristics have all been assessed using GE-137, the fluorescent-labeled analog of AH113804, in healthy volunteers and in patients at high risk of colorectal neoplasia (*17*).These initial studies in humans suggested that GE-137 was safe and that it may improve visualization of colonic polyps, which display a high level for c-Met (*17*).

In this study, we assessed ^{18}F-AH113804–driven PET for the early detection of locoregional tumor recurrence in a preclinical model of BLBC.

MATERIALS AND METHODS

Cell Culture

Human basal-like subtype breast cancer cells HCC1954 (CRL-2338) were obtained from the American Type Culture Collection and cultured in RPMI 1640 (Invitrogen) with 10% fetal calf serum (Bodinco BV) and 2 mM L-glutamine (Invitrogen) at 37°C in a fully humidified atmosphere containing 5% CO_2.

Western Blotting

Immunoblotting was performed as described by Ng et al. (*18*). Detection of bound antibody was with horseradish peroxidase–conjugated secondary antibodies and enhanced chemiluminescence (ThermoScientifc Fisher) with G:Box (Syngene).

Tumor Xenograft Model

All animal studies were performed in compliance with the U.K. Home Office Animals (Scientific Procedures) Act 1986. Female severe combined immunodeficient mice (17–19 g at the time of the first procedure; Charles River U.K.) were subcutaneously injected with 4×10^6 cells in 0.1 mL of a 1:1 mixture of medium and Matrigel (BD Biosciences) in the second right mammary fat pad. Tumor size was measured twice per week by caliper. The volume for the tumor was estimated as length × width^2/2. Further details on the tumor xenograft model are given in the supplemental methods (supplemental materials are available at http://jnm.snmjournals.org).

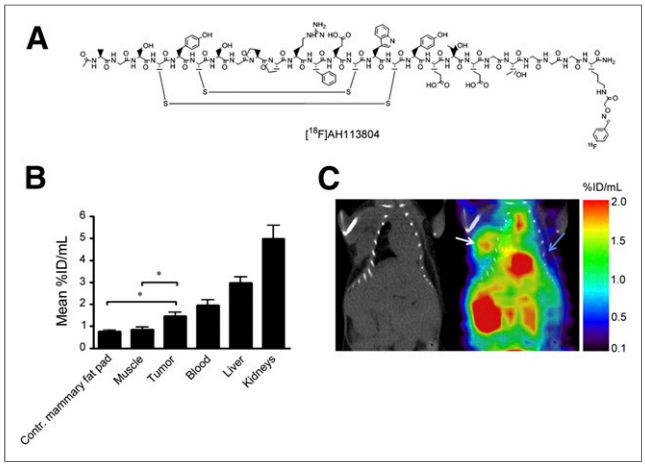

FIGURE 1. Biodistribution of ^{18}F-AH113804 and HCC1954 tumor. (A) Molecular structure of ^{18}F-AH113804. (B) Distribution of ^{18}F-AH113804 in selected organs and tissues in HCC1954 tumor xenografts 10 d after injection. Statistically significant differences were observed in uptake of ^{18}F-AH113804 in tumor versus muscle and contralateral (Contr.) side (Student *t* test, mean ± SEM, $n = 8$, $^*P < 0.05$). (C) CT and PET/CT images of a representative tumor-bearing mouse 10 d after injection demonstrates ^{18}F-AH113804 signal at tumor site (white arrow) but not at contralateral site (blue arrow).

Radiosynthesis of ^{18}F-AH113804

Synthesis of the peptide was as described in the supplemental section of Burggraaf et al. (*17*). Details of the radiosynthesis of ^{18}F-AH113804 are given in the supplemental methods.

CT and PET Imaging

Small-animal PET/CT imaging was performed using microPET P4 (Concorde) and microCAT II (ImTek Inc.) systems as described earlier (*19*). Each animal was injected intravenously with approximately 7 MBq (0.1 mL) of ^{18}F-AH113804. Further details of the imaging procedure are given in the supplemental methods.

Tumor and contralateral mammary fat pad uptake are presented as target–to–muscle retention ratio (TMRR). Further details are given in the supplemental methods.

Ex Vivo Tissue Analyses

Details of all ex vivo tissue analyses are given in the supplemental methods. These include histology of formalin-fixed, paraffin-embedded tumor and quadriceps muscle and ^{18}F-AH113804 autoradiography and immunofluorescence staining of snap-frozen tumor tissue.

Statistical Analysis

Unless otherwise stated, group averaged data are presented as mean ± SEM. The observed skewed distribution of TMRR measures was lessened by logarithmic transformation (supplemental methods). All statistical analyses were performed in R version 3.1.2 (R Project for Statistical Computing).

RESULTS

Synthesis of ^{18}F-AH113804

Total synthesis time on the automated platform was 49 min. For all synthesis runs, the decay-corrected end-of-synthesis yield was between 38% and 41%, with a radioactive concentration between 600 and 800 MBq/mL. The radiochemical purity was always greater than 90%, the chemical content between 15 and 20 μg/mL, and specific activity approximately 100 GBq/μmol for each test item.

c-Met Expression Level in HCC1954

Human c-Met protein expression level was assessed in HCC1954, compared with HT-29 (high c-Met–expressing) and U87 (moderate c-Met–expressing) cell line lysates. The data show upregulation of c-Met in the HCC1954 cell line (Supplemental Fig. 1). Burggraaf et al. assessed the specificity of GE-137, performing a competition study in HT-29 tumor–bearing mice, which showed a reduction in tumor uptake of GE-137 when coadministered with an excess of unlabeled peptide (*17*).

Tumor Targeting of ^{18}F-AH113804

The baseline uptake of ^{18}F-AH113804 (Fig. 1A) was assessed in 8 tumor-bearing animals using PET imaging at 10 d after tumor inoculation (Fig. 1B). Levels of radioactivity at 60 min after injection were 4.9 ± 0.6 percentage injected dose (%ID)/mL in kidney, 2.9 ± 0.3 %ID/mL in liver, and 2.0 ± 0.2 %ID/mL in blood. PET imaging (Fig. 1C) revealed a significant difference between the uptake of ^{18}F-AH113804 at the tumor site (1.5 ± 0.2 %ID/mL, white arrow), compared with both contralateral mammary fat pad (0.8 ± 0.1 %ID/mL, blue arrow) and muscle (0.8 ± 0.1 %ID/mL) at 60 min after injection. Ex vivo biodistribution studies, after PET imaging on day 50 after tumor resection, confirmed that ^{18}F-AH113804 accumulation in the tumor was

significantly higher than in the muscle (2.5 ± 0.6 vs. 0.9 ± 0.2 %ID/g at 70 min after injection, $n = 3$; $P < 0.05$; Supplemental Fig. 2).

Early-Stage Recurrent Tumor Growth Is First Detected with ^{18}F-AH113804, Later by CT, and Last by Palpation

After tumor resection 14–16 d after inoculation, 5 animals were found to exhibit recurrent tumor growth, confirmed by necropsy after final imaging. The remaining 3 animals did not exhibit any tumor regrowth (by caliper measurements). However, there was lack of correlation between tumor size by caliper and uptake of the tracer at the tumor site (Supplemental Fig. 3). Tissue from the site of injection for 1 of the nonrecurrent mice was stained. Negativity for tumor cells and human c-Met expression by immunohistochemistry was confirmed (Supplemental Fig. 4). In this case, the %ID/g in the region of interest was 0.6 (compared with the %ID/g at the contralateral site, which was 0.5).

Analysis of ^{18}F-AH113804 PET images provided evidence for the presence of locoregional recurrence from day 6 after resection in these 5 animals (Fig. 2A). There was some degree of variation in the uptake of radioactivity at the tumor site in individual animals on each study day (Supplemental Table 1). However, overall uptake on each day was comparable to that observed in the tumors before resection. The TMRR was significantly higher at the tumor resection site than the contralateral mammary fat pad on day 6 (2.7 ± 0.3 vs. 1.0 ± 0.3, $P < 0.001$; $n = 5$; Fig. 2B). Uptake of ^{18}F-AH113804 at the site of resection remained clearly visible in the PET images on subsequent days, with the TMRR significantly smaller in the contralateral mammary fat pad on day 13 (1.6 ± 0.2 vs. 0.9 ± 0.2, $P < 0.01$), day 20 (1.6 ± 0.1 vs. 0.9 ± 0.2, $P < 0.001$), and day 36 (1.5 ± 0.8 vs 0.9 ± 0.2, $P < 0.01$). At day 50 after tumor resection, the TMRR was also higher for the tumor site (1.7 ± 0.7) than for the contralateral mammary fat pad (1.0 ± 0.0), although this difference was not statistically significant. No specific ^{18}F-AH113804 retention was detected in the contralateral mammary fat pad, with levels of radioactivity in this region comparable to muscle tissue for all time points (Supplemental Fig. 5).

By day 20 after tumor resection, the mean tumor volume determined by CT measurement was approximately 7.0 ± 12.5 mm^3 (Fig. 3). Palpable tumor recurrence was detected from day 29 after tumor resection (Fig. 3A).

^{18}F-AH113804 Retention in Tumor Tissue Versus Systemic Clearance

Systemic clearance of ^{18}F-AH113804 was studied in selected tumor-bearing mice over the first 60 min after injection by dynamic PET imaging. Figure 4A shows the distribution of ^{18}F-AH113804 at 15 min (13–18 min) and 60 min (55–65 min) after injection. A decrease in ^{18}F-AH113804 signal in the major perfused organs and retention of ^{18}F-AH113804 at the tumor site (Fig. 4B) were observed.

Figure 4C displays the change in TMRR from 5 to 60 min after injection in relation to TMRR at 5 min after injection. Although the tumor TMRR continuously increased, TMRRs for the lungs, liver, heart, and others decreased.

Autoradiography and Immunohistochemical Analysis Confirm Is Observed AH113804 Accumulation in c-Met–Positive Tumor Tissues

A heterogeneous pattern of ^{18}F-AH113804 distribution was observed within the tumor, with viable tissue in the tumor periphery

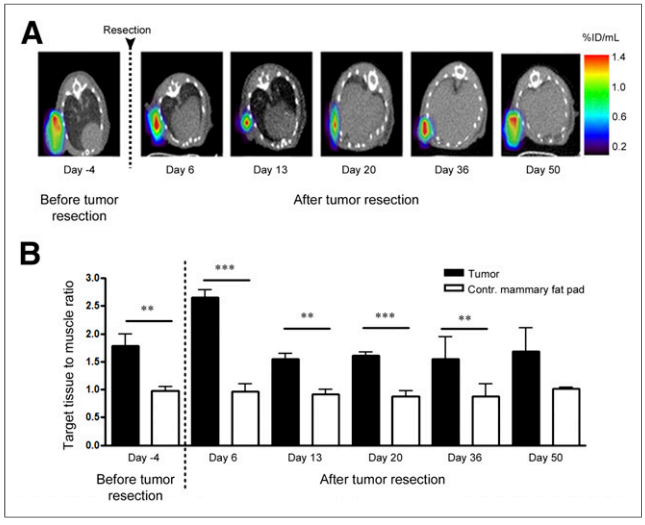

FIGURE 2. Early detection of tumor regrowth using ^{18}F-AH113804 for PET imaging. (A) PET/CT images of transverse section of representative tumor-bearing mouse, 4 d before tumor resection and at selected days after resection, show ^{18}F-AH113804 signal at tumor site at 60 min after injection. For clarity, PET signal only in region of interest is shown. (B) Target-to-muscle ratio in tumor and contralateral (Contr.) sites. Statistically significant differences between both sites observed at days 6, 13, 20, and 36 (Student *t* test, mean ± SEM; day 4 before resection: $n = 8$; days 6 and 13 after resection: $n = 5$; days 20 and 36: $n = 4$; day 50: $n = 3$). $^{**}P < 0.01$. $^{***}P < 0.001$.

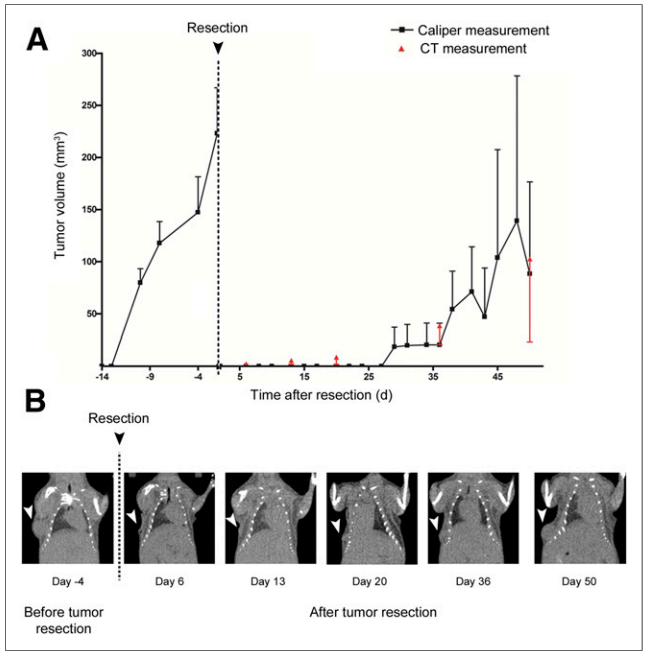

FIGURE 3. Detection of locoregional tumor recurrence via CT and caliper measurements. (A) Growth curve of mean tumor volume obtained from caliper and CT measurements of same group of animals, before and after primary tumor resection (mean ± SEM, $n = 5$ per study day, except days 20 and 36: $n = 4$, day 50: $n = 3$). (B) Coronal CT slices of representative tumor-bearing mouse before and after resection show presence (white arrowhead) and regrowth of tumor after resection. Tumor growth was observed by CT from day 20 onward.

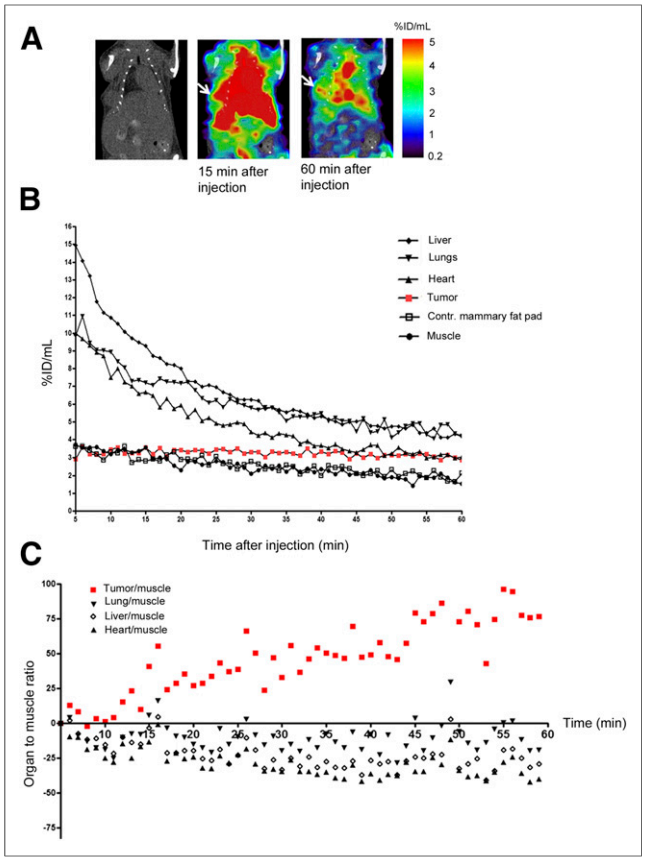

FIGURE 4. Biodistribution of ^{18}F-AH113804 in recurrent HCC1954 tumor–bearing mouse. (A, left) Representative CT image of HCC1954 xenograft mouse, acquired at day 36 after resection. Recurrent tumor observed (white arrowhead). (A, middle and right) PET/CT at 15 and 60 min after injection of ^{18}F-AH113804, with retained radioactivity in tumor visible by 60 min after injection. (B) Dynamic region-of-interest analysis of PET/CT shows constant concentration at tumor site but steady decline in all other organs (n = 1). (C) Data from B normalized to first time point show relative change, with clear increase for tumor (n = 1). Contr. = contralateral.

exhibiting a positive signal whereas the central tumor regions exhibited only low activity (Fig. 5A). Hematoxylin and eosin (H&E) staining and immunohistochemistry of consecutive tumor slides revealed a large number of c-Met–positive tumor cells (Fig. 5B, left and right panels, respectively). Both recurrent and primary tumors showed necrotic areas in H&E devoid also of c-Met (immunohistochemistry) and displaying low ^{18}F-AH113804 uptake (Supplemental Figs. 6 and 7).

Ex Vivo Histology Correlates with PET Images

After immunofluorescent staining (Fig. 6A), c-Met expression levels were quantified across whole tumor slides (Fig. 6B). A significant correlation was found between c-Met expression and in vivo PET (r = 0.82, P = 0.023, n = 7), suggesting ^{18}F-AH113804 signal in tumor at 60 min after injection to be representative of c-Met expression. A similar correlation was observed between c-Met expression determined by immunohistochemistry and ^{18}F-AH113804 signal in vivo (r = 0.83, P = 0.0015) (Supplemental Fig. 8).

In addition, it was found that the variation in the c-Met expression levels observed across the tumor samples (displayed in Fig. 6B) was due to the tumor size. Indeed, a correlation (r = 0.83, P = 0.0005)

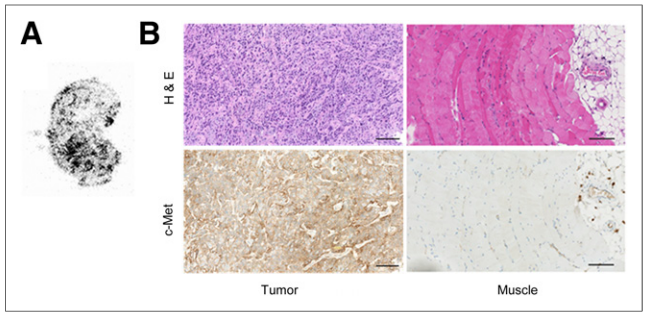

FIGURE 5. Autoradiography and immunohistochemistry demonstrate ^{18}F-AH113804 retention in c-Met–positive HCC1954 tumor tissue. (A) Autoradiography performed ex vivo on resected tumor confirms retention of ^{18}F-AH113804 radiotracer in tumor tissues. Heterogeneous distribution of tracer within tumor section could be observed, not visible at limited spatial resolution of PET imaging. (B) H&E staining (upper) and c-Met immunostaining (lower) of paraffin-embedded tumor and control skeletal muscle tissue (left and right columns, respectively). H&E staining reveals large, mitotic and disorganized phenotype characteristic of tumor cells, whereas immunohistochemistry reveals membranous c-Met staining in these cells. Scale bars = 100 μm.

was identified between the total c-Met intensity level and the surface area of the tumor sample (Supplemental Fig. 9).

DISCUSSION

Early detection and identification of tumor relapse enables improved locoregional recurrence control resulting in an increased quality of life and better overall survival for BC patients (*20*). Current surveillance guidelines have been shown to be less effective in the detection of locoregional recurrence than the more expensive, yet more sensitive, approaches such as MRI or radionuclide imaging (SPECT, PET) (*13,14*). It is believed that either

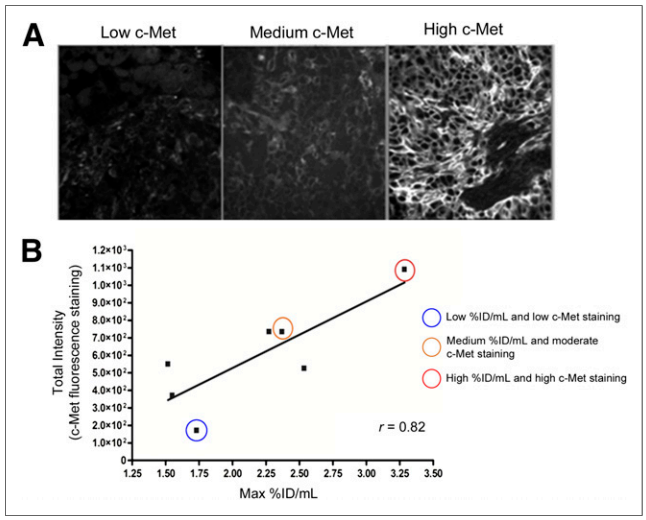

FIGURE 6. Uptake of ^{18}F-AH113804 correlates with c-Met expression level in corresponding resected tumor samples. (A) Immunofluorescent staining for c-Met in resected tumor samples (day 14, n = 7). Low, medium, and high c-Met staining examples highlighted in B. (B) Positive correlation is found between maximum (Max) %ID/mL of tumor regions of interest from in vivo PET images and c-Met protein expression level from immunofluorescent staining in same tumors after resection. Pearson correlation coefficient = 0.82 (P < 0.05, n = 7).

individually or as a companion test for established diagnostic approaches, targeted molecular imaging of specific tumor markers bears the potential to positively change BC follow-up, especially in patients presenting with a high risk of relapse, such as BLBC patients (*20,21*).

^{18}F-AH113804 is known to have a high affinity for human c-Met, as demonstrated in studies by Evans et al., in which the in vivo affinity of ^{18}F-AH113804 was determined via receptor blocking in HT-29 xenograft tumor mouse models (*22*). ^{18}F-AH113804 clears quickly from plasma and nontarget tissues (such as liver, lungs, and heart), allowing for high-contrast imaging after injection and improving the sensitivity for tumor detection, as confirmed by PET imaging in this study.

Our study shows that ^{18}F-AH113804–driven PET imaging allowed for early detection of locoregional tumor recurrence in HCC1954 tumor–bearing mice after surgery. ^{18}F-AH113804 uptake and retention in the lungs and heart, reflecting the nonspecific blood-pool distribution of ^{18}F-AH113804, decreased constantly over the observation period. In contrast, a constant signal was observed within the region of tumor regrowth, indicative of specific accumulation of ^{18}F-AH113804 due to target binding. ^{18}F-AH113804 allows for excellent tissue penetration, and the in vivo PET imaging revealed a satisfactory tumor–to–nontarget (muscle) tissue ratio from 1 h after injection.

We were able to detect statistically significant differences in tumor uptake compared with contralateral mammary fat pad at days 6, 13, 20, and 36 after tumor resection. The lack of statistical significance at the latter time points is most likely due to the lower, inhomogeneous distribution of radioactivity in the tumors. PET images from some of those recurrent tumor-bearing animals (images not shown) showed evidence of peripheral uptake only, indicative of necrosis in the tumor core.

Currently ^{18}F-FDG is used in PET diagnostics for detection and staging in cancer. Numerous studies have revealed that other, more target-specific tracers would be beneficial for the detection of locoregional recurrence (*23*). In a study of patients with breast cancer, it was shown that tumor size was an important factor when correctly diagnosing patients (*24*). A review of 111 patients showed that a tumor size of less than 10 mm was a significant predictor of a false-negative ^{18}F-FDG PET result (*16*). In our study, a specific signal from ^{18}F-AH113804 could be detected, even when the recurrent tumor was not yet observable via CT. A previous study by Cullinane et al. found 3′-deoxy-3′-^{18}F-fluorothymidine (^{18}F-FLT) to be superior over ^{18}F-FDG in assessing the effect of the c-Met inhibitor crizotinib in human glioblastoma and human gastric cancer preclinical models (*25*). When tumor size decreased within 1 wk of treatment, ^{18}F-FDG uptake remained unchanged whereas ^{18}F-FLT PET showed a marked decrease in uptake. ^{18}F-FLT is reflective of cell proliferation and as such was indicative of tumor therapy response. Still, the use of ^{18}F-FLT as a marker for proliferation has been heavily debated, with reports suggesting that results should be viewed with caution (*26*). Such studies denote the importance of targeting radiotracers such as ^{18}F-AH113804 for accurate tumor detection and patient monitoring.

Our study demonstrates correlation between c-Met from the tumor samples and the maximum uptake (%ID/mL) from ^{18}F-AH113804 at those sites in the corresponding PET images. A recent study using an optical analog of AH113804 (GE-137) also showed a good concordance between the expression of c-Met and the optical signal detected (*17,27*).

Other groups have investigated the use of both monoclonal antibodies and anticalins as probes for c-Met imaging. ^{89}Zr-db-/^{76}Br-ornartuzumab and ^{89}Zr-PRS-110 were developed and assessed for visualization of c-Met–positive tumors in preclinical models (*28,29*). Optimal imaging time points were identified to be between 2 and 5 d after tracer administration, thus hampering potential routine clinical use as diagnostic agents. In contrast, the biodistribution of ^{18}F-AH113804 permitted early imaging after tracer administration. Similarly, Li et al. explored the use of c-Met–targeting scFv-cys dimers in non–small cell lung cancer xenografts. Despite showing very high affinity for c-Met, good-contrast immune-PET imaging was achieved only at 20 h after injection (*30*).

The ubiquity of c-Met dysregulation in malignant disease and its known influence on tumor progression make c-Met an attractive target for diagnostic targeting and therapeutic intervention in multiple cancer types. Phase II and III clinical studies, evaluating c-Met inhibition in gastroesophageal cancer, lung cancer, and hepatocellular carcinoma, have shown encouraging results with a clear benefit for the individual patient (*4,31,32*).

It is hypothesized for BC, as well as for those cancer types that react more favorably to c-Met inhibition, that stratification of patients according to aberration in the c-Met axis resulting in target overexpression would strongly increase the efficiency of targeted treatment.

^{18}F-AH113804–mediated PET signals proved to reflect the c-Met expression in individual tumors in our BC model, suggesting that this tracer could also serve as such a companion diagnostic for patient selection and for therapeutic purposes. Future studies to evaluate this utility are required.

CONCLUSION

This study demonstrated that ^{18}F-AH113804 PET provides a new diagnostic tool for the detection of c-Met–expressing primary tumor and has potential utility for the detection of locoregional recurrence from an early stage. Further preclinical work is warranted to determine whether ^{18}F-AH113804 uptake in the regrowth provides a useful predictive tool for anti–c-Met therapeutic intervention.

DISCLOSURE

The costs of publication of this article were defrayed in part by the payment of page charges. Therefore, and solely to indicate this fact, this article is hereby marked “advertisement” in accordance with 18 USC section 1734. This work was supported by a MRC UK/GE Healthcare CASE studentship, MR/L001640/1, a FP7-HEALTH-2010 grant ‘Imagint’ (no. 259881), CR-UK/EPSRC funding for the KCL-UCL CCIC (C1519/A10331, C1519/A16463), an endowment fund from Dimbleby Cancer Care to KCL, and a Breakthrough Breast Cancer fund. No other potential conflict of interest relevant to this article was reported.

ACKNOWLEDGMENTS

We thank GE Healthcare for providing ^{18}F-AH113804 and for providing access to their laboratory facilities and staff. In particular, we thank Joanne Nesbitt, Rochelle Lear, David Gendle, and Chris Beazley (all GE Healthcare at the time of study) for excellent technical support. We also thank Sven Macholl and Mark

Battle (both GE Healthcare at the time of study) for excellent technical and intellectual support. We thank Anthony Cheung and Fabian Flores-Borja (both KCL) for preparatory experiments.

REFERENCES

1. Birchmeier C, Birchmeier W, Gherardi E, et al. Met, metastasis, motility and more. *Nat Rev Mol Cell Biol.* 2003;4:915–925.
2. Bean J, Brennan C, Shih JY, et al. Met amplification occurs with or without T790M mutations in EGFR mutant lung tumors with acquired resistance to gefitinib or erlotinib. *Proc Natl Acad Sci USA.* 2007;104:20932–20937.
3. Rong S, Segal S, Anver M, et al. Invasiveness and metastasis of NIH 3T3 cells induced by Met-hepatocyte growth factor/scatter factor autocrine stimulation. *Proc Natl Acad Sci USA.* 1994;91:4731–4735.
4. Study evaluating the safety and efficacy of onartuzumab (Metmab) and/or bevacizumab in combination with paclitaxel in patients with metastatic, triple negative breast cancer. ClinicalTrials.gov website. https://clinicaltrials.gov/ct2/show/NCT01186991. Updated December 31, 2015. Accessed January 28, 2016.
5. Bandla S, Pennathur A, Luketich JD, et al. Comparative genomics of esophageal adenocarcinoma and squamous cell carcinoma. *Ann Thorac Surg.* 2012;93:1101–1106.
6. Gastaldi S, Comoglio PM, Trusolino L. The Met oncogene and basal-like breast cancer: another culprit to watch out for? *Breast Cancer Res.* 2010;12:208–217.
7. Dent R, Trudeau M, Pritchard KI, et al. Triple-negative breast cancer: clinical features and patterns of recurrence. *Clin Cancer Res.* 2007;13:4429–4434.
8. Lowery AJ, Kell MR, Glynn RW, et al. Locoregional recurrence after breast cancer surgery: a systematic review by receptor phenotype. *Breast Cancer Res Treat.* 2012;133:831–841.
9. Pogoda K, Niwinska A, Murawska M, et al. Analysis of pattern, time and risk factors influencing recurrence in triple-negative breast cancer patients. *Med Oncol.* 2013;30:388–395.
10. Eiermann W, Vallis KA. Locoregional treatments for triple-negative breast cancer. *Ann Oncol.* 2012;23(suppl 6):vi30–vi34.
11. Wapnir IL, Anderson SJ, Mamounas EP, et al. Prognosis after ipsilateral breast tumor recurrence and locoregional recurrences in five national surgical adjuvant breast and bowel project node-positive adjuvant breast cancer trials. *J Clin Oncol.* 2006;24:2028–2037.
12. Voogd AC, van Oost FJ, Rutgers EJ, et al. Long-term prognosis of patients with local recurrence after conservative surgery and radiotherapy for early breast cancer. *Eur J Cancer.* 2005;41:2637–2644.
13. Montgomery DA, Krupa K, Cooke TG. Alternative methods of follow up in breast cancer: a systematic review of the literature. *Br J Cancer.* 2007;96:1625–1632.
14. Schneble EJ, Graham LJ, Shupe MP, et al. Current approaches and challenges in early detection of breast cancer recurrence. *J Cancer.* 2014;5:281–290.
15. Schneble EJ, Graham LJ, Shupe MP, et al. Future directions for the early detection of recurrent breast cancer. *J Cancer.* 2014;5:291–300.
16. Kumar R, Chauhan A, Zhuang H, et al. Clinicopathologic factors associated with false negative FDG-PET in primary breast cancer. *Breast Cancer Res Treat.* 2006;98:267–274.
17. Burggraaf J, Kamerling IM, Gordon PB, et al. Detection of colorectal polyps in humans using an intravenously administered fluorescent peptide targeted against c-Met. *Nat Med.* 2015;21:955–961.
18. Ng T, Shima D, Squire A, et al. PKCα regulates beta1 integrin-dependent cell motility through association and control of integrin traffic. *EMBO J.* 1999;18:3909–3923.
19. Battle MR, Goggi JL, Allen L, et al. Monitoring tumor response to antiangiogenic sunitinib therapy with ^{18}F-fluciclatide, an ^{18}F-labeled $\alpha_V\beta_3$-integrin and $\alpha_V\beta_5$-integrin imaging agent. *J Nucl Med.* 2011;52:424–430.
20. Meyers MO, Klauber-Demore N, Ollila DW, et al. Impact of breast cancer molecular subtypes on locoregional recurrence in patients treated with neoadjuvant chemotherapy for locally advanced breast cancer. *Ann Surg Oncol.* 2011;18:2851–2857.
21. Sohn YJ, Jang JS, Choi SR, et al. Early detection of recurrence after endoscopic treatment for early gastric cancer. *Scand J Gastroenterol.* 2009;44:1109–1114.
22. Evans PBM, Getvoldsen G, McRobbie G, et al. Nonclinical tumor efficacy studies of [^{18}F]AH113804, a novel PET imaging agent with high affinity for the human c-Met receptor [abstract]. *Cancer Res.* 2012;72:357.
23. Gaeta CM, Vercher-Conejero JL, Sher AC, et al. Recurrent and metastatic breast cancer PET, PET/CT, PET/MRI: FDG and new biomarkers. *Q J Nucl Med Mol Imaging.* 2013;57:352–366.
24. Vallabhajosula S. ^{18}F-labeled positron emission tomographic radiopharmaceuticals in oncology: an overview of radiochemistry and mechanisms of tumor localization. *Semin Nucl Med.* 2007;37:400–419.
25. Cullinane C, Dorow DS, Jackson S, et al. Differential ^{18}F-FDG and 3′-deoxy-3-^{18}F-fluorothymidine PET responses to pharmacologic inhibition of the c-Met receptor in preclinical tumor models. *J Nucl Med.* 2011;52:1261–1267.
26. McKinley ET, Ayers GD, Smith RA, et al. Limits of [^{18}F]-FLT PET as a biomarker of proliferation in oncology. *PLoS One.* 2013;8:e58938.
27. Liu S, Zheng Y, Volpi D, et al. Toward operative in vivo fluorescence imaging of the c-Met proto-oncogene for personalization of therapy in ovarian cancer. *Cancer.* 2015;121:202–213.
28. Jagoda EM, Lang L, Bhadrasetty V, et al. Immuno-PET of the hepatocyte growth factor receptor Met using the 1-armed antibody onartuzumab. *J Nucl Med.* 2012;53:1592–1600.
29. Terwisscha van Scheltinga AG, Lub-de Hooge MN, Hinner MJ, et al. In vivo visualization of MET tumor expression and anticalin biodistribution with the MET-specific anticalin ^{89}Zr-PRS-110 PET tracer. *J Nucl Med.* 2014;55:665–671.
30. Li K, Tavare R, Zettlitz KA, et al. Anti-MET immunoPET for non-small cell lung cancer using novel fully human antibody fragments. *Mol Cancer Ther.* 2014;13:2607–2617.
31. A study of foretinib in patients with recurrent/metastatic breast cancer (IND197). ClinicalTrials.gov website. https://clinicaltrials.gov/ct2/show/NCT01147484. Updated February 13, 2015. Accessed January 28, 2016.
32. Cabozantinib for metastatic triple negative BrCa. Institute D-FC. ClinicalTrials.gov website. https://clinicaltrials.gov/show/NCT01738438. Updated November 17, 2015. Accessed January 28, 2016.